PROCEEDINGS OF SPIE

LO WFS of MAORY: performance and sky coverage assessment

C. Plantet, G. Agapito, C. Giordano, L. Busoni, M. Bonaglia, et al.

SPIE.

LO WFS of MAORY: performance and sky coverage assessment

C. Plantet[a], G. Agapito[a], C. Giordano[a], L. Busoni[a], M. Bonaglia[a], S. Esposito[a], C. Arcidiacono[b], F. Cortecchia[b], P. Ciliegi[b], E. Diolaiti[b], M. Bellazzini[b], R. Ragazzoni[c], and P. Feautrier[d]

[a]INAF, Osservatorio **Astrofisico** di Arcetri, Largo Enrico Fermi 5, 50125 Firenze, Italy
[b]INAF Osservatorio Astrofisico e scienza dello Spazio di Bologna (OAS) via Gobetti 93/3 40129 Bologna
[c]INAF, Osservatorio Astronomico di Padova, Vicolo dell'Osservatorio 5, 35122 Padova, Italy
[d]Institut de Planétologie et d'Astrophysique de Grenoble, 414 Rue de la Piscine, Domaine Universitaire, 38400 St-Martin d'Hères, France

ABSTRACT

MAORY is the Multi-Conjugate Adaptive Optics module for the European ELT. It will provide a wide-field correction for the first-light instrument MICADO. The Low-Order wavefront modes will be sensed on 3 Natural Guide Stars with Shack-Hartmann Wavefront Sensors, so-called the LO WFS. In the presented work, we focus on the numerical study of the main aspects that depend on the LO WFS design and operational use: low-order sensing performance and sky coverage.

Keywords: Adaptive optics, Wavefront sensing, Multi-Conjugate Adaptive Optics, MAORY

1. INTRODUCTION

MAORY is the Multi-Conjugate Adaptive Optics (MCAO) module for the European ELT.[1] It will provide a >30% Strehl Ratio (SR) in K-band on the 53x53" Field of View (FoV) of the first-light instrument MICADO,[2] with a 50% sky coverage. The AO system itself, as a baseline, will consist of 2 Deformable Mirrors (DM), 6 Laser Guide Star (LGS) Wavefront Sensors (WFS) and 3 couples of Natural Guide Star (NGS) WFS. The latter form the LOR (Low Order and Reference) module, for fast low-order sensing (up to astigmatism) and slow truth sensing. Both WFS modules use Shack-Hartmann (SH) sensors. In this paper, we present the numerical simulations and performance analysis of the LO sensors, as well as a first assessment of sky coverage. This work relies on full end-to-end simulations of the MCAO system, as well as analytical and semi-analytical formulas for the computation of the different error terms. The first goal is to choose the conceptual design parameters of the LO sensors: number of subapertures, sensing band and pixel size. The second goal is to determine two main aspects of the MCAO system: technical FoV size and number of DMs. We first focus on the design of the LO sensors, in section 2, and then show the first sky coverage results in section 3.

2. LO WFS DESIGN STUDY

The goal of this section is compute the performance of the LO sensors and to choose their main design parameters, i.e. the number of subapertures (2×2 to 5×5), the sensing spectral band (H or R+I) and the pixel scale.

We evaluate here the performance on LO given by the possible configurations. This work is partially done using phase screens provided by ESO, using the simulation tool OCTOPUS.[3] These phase screens correspond to residuals of a LGS MCAO, and have the following characteristics:

- ESO median profile, seeing: 0.73" (at zenith and at 500 nm).

Further author information:
C.P.: E-mail: plantet@arcetri.astro.it, Telephone: +39 0552752289

- Zenith angle: 30°.

- 1 post-focal DM conjugated at 12.7 km, with a 2-meter pitch.

- 6 LGSs uniformly distributed on a 1' radius.

- 10 lines of sight: 1 on axis, 3 at 45", 3 at 70" and 3 at 85".

- 5 independent realizations of 500 frames at 500 Hz.

- Low orders corrected with the LGSs (replaced by turbulent modes in our simulations).

- Limitations: No spot elongation, high flux regime.

The other limitations of this analysis are:

- No windshake or vibrations from other sources

- We consider only the LO residuals on a single NGS, the tomographic error is not included.

2.1 LO error computation

We compute here the expected LO residuals as a function of the incoming flux. We first evaluate the error on the slopes, for a computation with a Weighted Center of Gravity (WCoG). We then propagate this error in the loop control. We focus here on the noise error to determine the best configuration. We also verify that it is the determining error term for the configuration choice by evaluating the aliasing effects on the estimation.

2.1.1 Slope computation

The WCoG is defined by:

$$S_x = \frac{\sum_k x_k w_k I_k}{\sum_k w_k I_k} \tag{1}$$

with S_x the slope in X, k the pixel number, x the X coordinate, w the weighting function and I the image.

At low flux, the denominator of the WCoG can be very close to 0, making the variance of the slopes extremely high and unpredictable. In practice, we can consider two solutions:

- Thresholding at 0 (all values under 0 are put to 0): the statistical behaviour of the slopes with a threshold is also hard to predict, whether in terms of variance or bias.

- Constant denominator (e.g. the mean flux per subaperture): this solution is much simpler to evaluate and is unbiased (or biased by a constant factor).

In the following, we study the behavior of the first solution, that is used in our simulations, with respect to noise.

2.1.2 Slope noise error and bias

The error variance on the WCoG measurement is (without thresholding or using a constant denominator):

$$\sigma^2_{WCoG} = \frac{\sum_k x_k^2 w_k^2 \sigma_k^2}{\left(\sum_k w_k I_k\right)^2} \tag{2}$$

with σ_k^2 the noise variance on each pixel (photon noise from the PSF + detector noise + background noise). In the case of thresholding at 0, the error variance becomes:

$$\sigma^2_{WCoG} = \frac{\sum_k x_k^2 w_k^2 \sigma_{k,thr}^2}{\left(\sum_k w_k \mu_{k,thr}\right)^2} \tag{3}$$

with $\mu_{k,thr} = f_k + \sigma_e\varphi(-f_k/\sigma_e)$ and $\sigma^2_{k,thr} = Ff_k + \sigma^2_e \left[1 - \Phi(-f_k) - \varphi(-f_k/\sigma_e)^2\right] - f_k\sigma_e\varphi(-f_k/\sigma_e)$ the approximated mean and variance of the addition of a Poisson noise of flux f_k and a zero-mean Gaussian noise of variance σ^2_e, thresholded at 0 (see Appendix A). Here f_k is the total flux per pixel (with background if not removed) and σ_e is the read-out noise. F is the excess noise factor, and we use the following functions: $\varphi(x) = \frac{1}{\sqrt{2\pi}}e^{-\frac{x^2}{2}}$ and $\Phi(x) = \frac{1}{2}\left[1 + \mathrm{erf}\left(\frac{x}{\sqrt{2}}\right)\right]$, erf being the error function.

The values $\mu_{k,thr}$ and $\sigma^2_{k,thr}$ are actually the mean and variance of a zero-mean Gaussian noise truncated at $-f_k$, to which we added the mean and variance of the photon noise for the flux f_k. The mean of the thresholded WCoG, that will help us compute the bias, is then:

$$\mu_{WCoG,thr} = \frac{\sum_k x^2_k w^2_k \mu_{k,thr}}{\sum_k w_k \mu_{k,thr}} \tag{4}$$

We compare the slope error of the 2 methods described in the previous section with the theoretical error using Monte-Carlo simulations in Fig. 1, for an input slope always at 0. The sensor is a SH 2×2 in infrared (IR), i. e. in H band, or in visible, i. e. in R+I bands. For the constant denominator, we have a perfect match between simulations and theory. The match is a little less good for the thresholded WCoG, with an error of maximum 20%, but typically lesser or equal to 10% for cases that are considered here, which we assume sufficient for the present analysis.
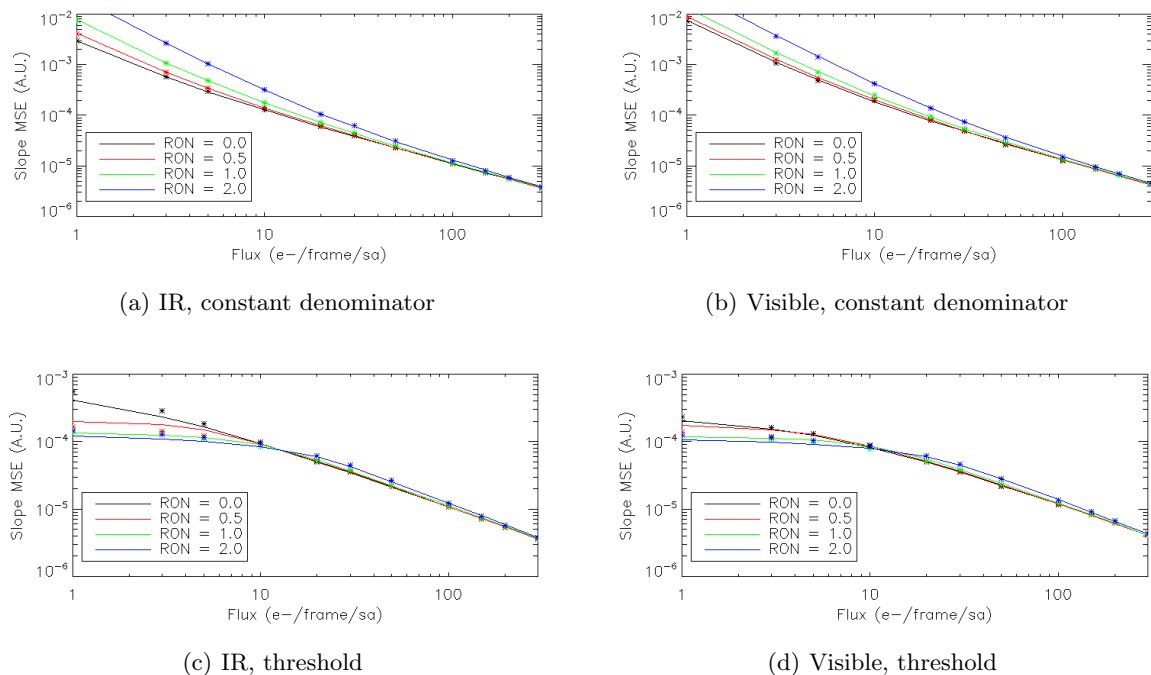

(a) IR, constant denominator

(b) Visible, constant denominator

(c) IR, threshold

(d) Visible, threshold

Figure 1. Slope error variance as a function of flux for different values of RON, with a constant denominator (top) or a threshold at 0 (bottom). The pupil sampling is 2×2 and the FoV size is 50 pixels. Top and bottom left: diffraction-limited (spot FWHM = 17 mas) IR sensor with 10 mas pixels, FWHM of WCoG = 2 pixels, background + dark = 0.2 e-/pixel. Top and bottom right: seeing-limited (spot FWHM = 0.2") visible sensor with 100 mas pixels, FWHM of WCoG = 2 pixels, background + dark = 0.53 e-/pixel. Solid lines: theory. Symbols: simulations.

In order to quantify the biasing effect of the threshold, we also plot in Fig. 2 the "bias factor", i.e. the ratio between the estimated slope and the input slope, as a function of flux. The match between the simulations and the theory is satisfying as well here. We observe a strong dependence of the bias with respect to the flux. This will have an impact on the transfer functions of the closed loop (see section 2.1.3). The saturation around 0.5

corresponds to the normal bias factor of the WCoG in our conditions, as stated in a paper by Thomas et al.[4] (using Nw = Nt in Thomas's equations).
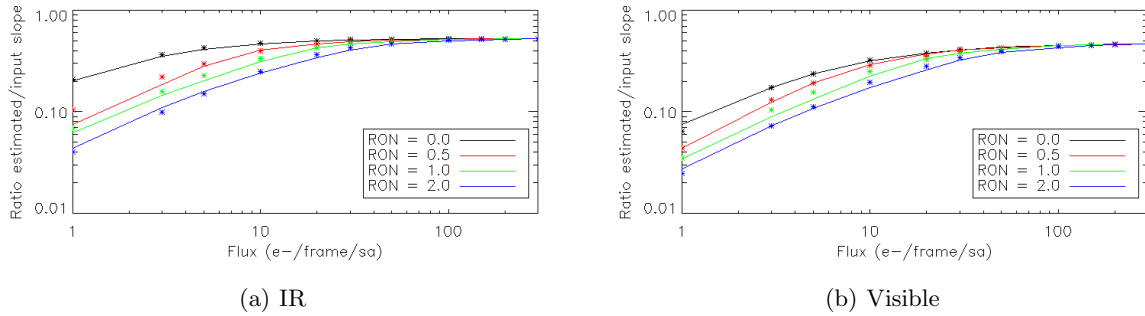

(a) IR

(b) Visible

Figure 2. Ratio between the measured slope and the input slope with the same parameters as in Fig. 1. The input slope is 0.5 pixel. Left: infrared sensor. Right: visible sensor. Solid line: theory, Symbols: simulations.

2.1.3 Closed-loop noise error

The residual due to noise in closed loop, in mean square error (MSE), is computed as follows:

$$\text{MSE} = \int_0^{\infty} |\text{NTF}|^2 \, \text{PSD}_{\text{noise}} \, df \tag{5}$$

with NTF the noise transfer function and $\text{PSD}_{\text{noise}}$ the noise temporal power spectrum density. In practice, we do not have the PSD or transfer function for all frequencies, so the integration is made on an interval Δf. The NTF, taking into account the bias in the slope estimation, is:

$$\text{NTF}(z) = \frac{-Gz^{-d}}{1 - z^{-1} + Gbz^{-d}} \tag{6}$$

where G is the integrator gain, z is the Z-transform variable and b the bias factor. The noise PSD is white, and its value is:

$$\text{PSD}_{\text{noise}} = \frac{1}{\Delta f} \text{Tr}(RR^t)\sigma^2_{WCoG,thr} \tag{7}$$

with R the reconstruction matrix, computed from a geometrical Shack-Hartmann here.

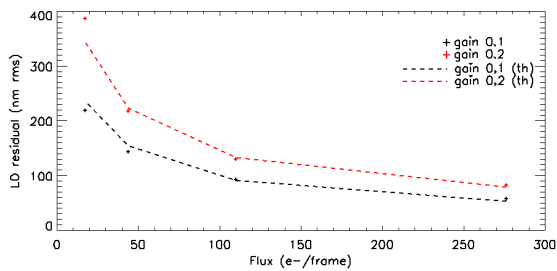### 2.1.4 Comparison with simulations

To confirm our analysis, we do a first comparison of the theoretical error with Single-Conjugated AO simulations including noise only. The fluxes considered here are in agreement with a preliminary sky coverage analysis, where the limiting flux is evaluated at approximately 100 e-/frame in infrared or in visible (at 500 Hz). We plot in Fig. 3 the theoretical and simulations residuals due to noise for different configurations in infrared. The image is diffraction-limited, but with a factor 0.11 on the flux, corresponding to the Strehl ratio in H band at 70" off-axis (i.e. an input flux of 100 e-/frame corresponds to 100/4×0.11 = 2.75 e-/frame/subaperture on the SH 2×2). We have a good overall match for all configurations. At very low flux, we lose accuracy, but the match is satisfying (typically a few nm difference, 15 nm at max) around 100 e-/frame, which is our zone of interest. The same is done in visible (Fig. 4), with a good match as well for the 2×2 and 3×3, and a loss of accuracy below 100 e-/frame on the 4x4, that is being investigated. In this case, to simulate the atmosphere widening effect on the PSF, we convolved the diffraction-limited PSF by a Gaussian kernel of 0.2" (FWHM measured from ESO phase screens at 70" off-axis with low orders removed).
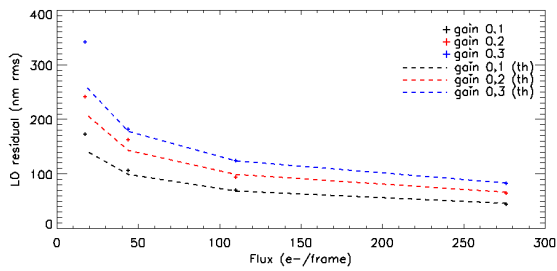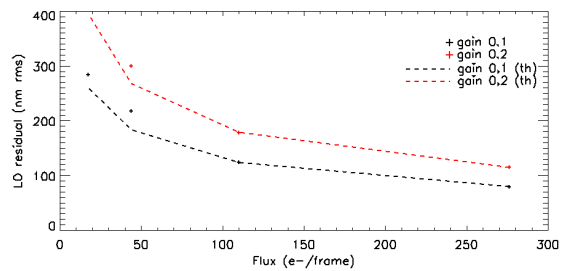
(a) 2×2 ; pix = 10 mas ; FWHM = 2
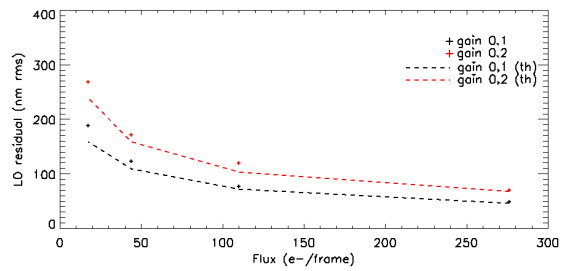
(b) 2×2 ; pix = 10 mas ; FWHM = 4

(c) 2×2 ; pix = 20 mas ; FWHM = 2

(d) 3×3 ; pix = 20 mas ; FWHM = 2
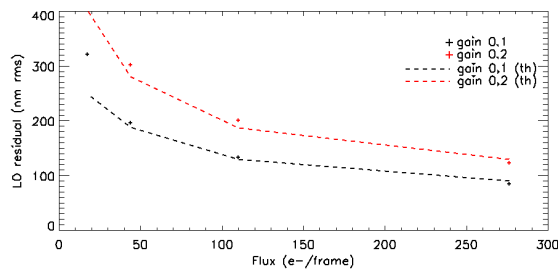
(e) 4×4 ; pix = 20 mas ; FWHM = 2

Figure 3. Comparison of theoretical residual (dashed lines) and residual found in simulations (symbols) for different configurations in infrared, with only noise. The title of each plot indicates the pupil sampling, the pixel scale and the FWHM of the WCoG (in pixels). The Strehl ratio considered here is 0.11, meaning that the flux is scaled by 0.11 before making the image. Readout noise: 0.8 e-. Dark current: 0.04 e-/pixel/frame. Background: 0.157 e-/frame/pixel for the SH 2×2 and 10 mas pixel (scaled with pupil sampling and pixel size in other configurations).

(a) 2×2

(b) 3×3

(c) 4×4

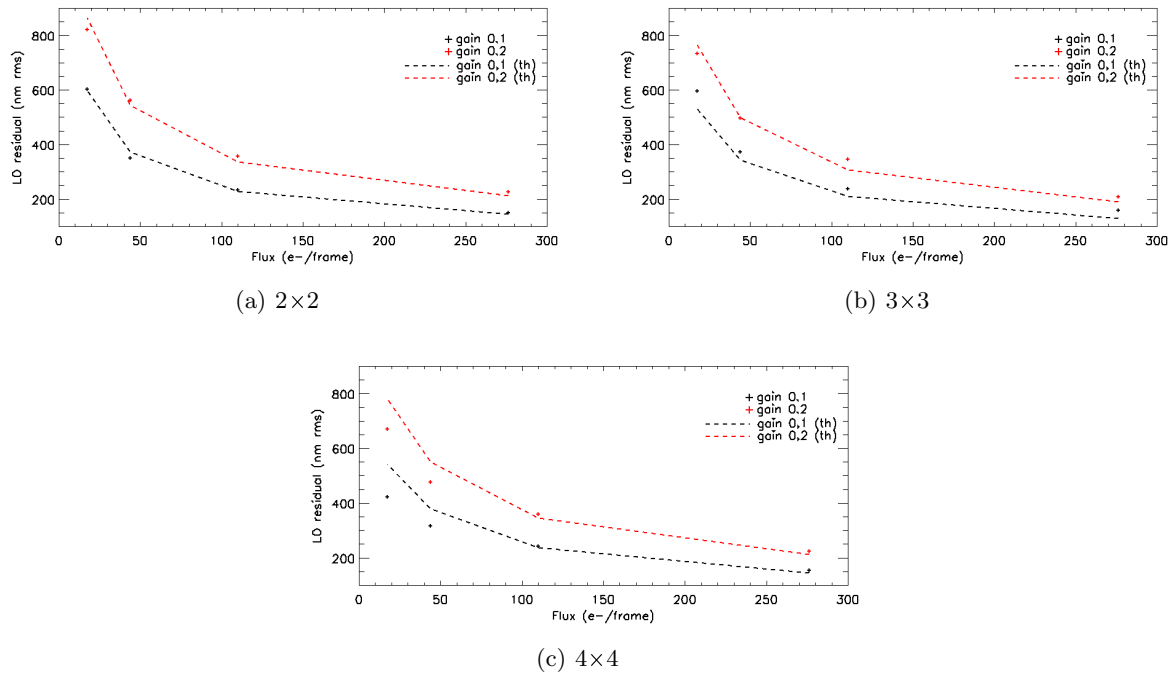Figure 4. Comparison of theoretical residual (dashed lines) and residual found in simulations (symbols) for different configurations in visible, with only noise. The title of each plot indicates the pupil sampling. The pixel scale is 100 mas, and the FWHM of the weighting is 2 pixels. The spot is here convolved by a Gaussian kernel of FWHM = 0.2" to simulate the widening effect of the atmosphere. Readout noise: 0.375 e-. Dark current: 0.006 e-/pixel/frame. Background: 0.387 e- /frame/pixel for the SH 2×2, scaled with the number of subapertures.

2.1.5 Aliasing

To verify that we can consider the noise error only for the comparison of configurations, we evaluate the aliasing error as a function of pupil sampling. The modes that are not estimated by the sensor give a slope signal that degrades the estimation of LO modes. The slope model (without noise) can be written as follows:

$$s = D_\infty A_{res} \tag{8}$$

with s the vector of slopes, D_∞ the interaction matrix with an infinite number of modes, and A_{res} the vector of residual modes coefficients (infinite as well). When estimating N modes, we apply a reconstructor R_N so that:

$$\hat{A} = R_N s = C_{alias} A_{res} \tag{9}$$

with $C_{alias} = R_N D_\infty$. C_{alias} is called here the "aliasing matrix". We estimate it with an interaction matrix D_M, where M >> 1 (4099 in the following). This interaction matrix is computed using a WCoG (FWHM = 2 pixels in this case), to reflect the behavior of the slope computation in operational conditions. If A_{res} is known, we can then compute the RMS error due to aliasing by using the following relation:

$$< \hat{A}\hat{A}^t > = C_{alias} < A_{res}A_{res}^t > C_{alias}^t \tag{10}$$

The matrix $< A_{res}A_{res}^t >$ is considered diagonal and its diagonal is the modal PSD of the residuals. We compute it with the phase screens given by ESO. In Fig. 5, we plot the total aliasing error on the different estimated modes (tip/tilt, focus, astigmatism) for all SH configurations, with a high-order PSD computed at 70" off-axis. All configurations estimate no more than 5 modes, to keep noise propagation to a minimum.
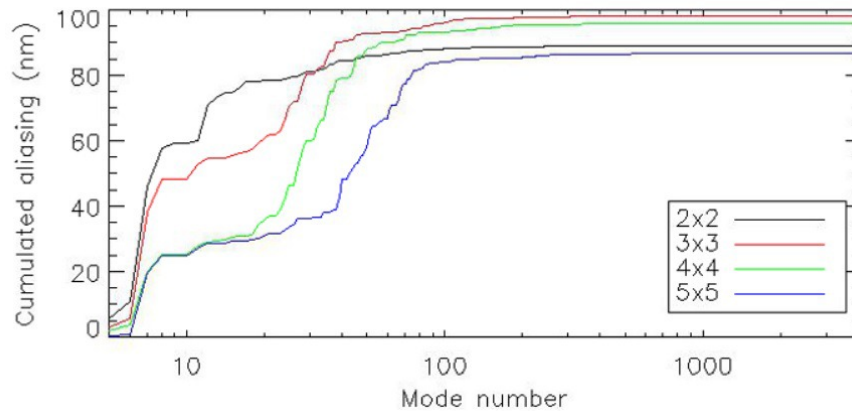
Figure 5. Cumulated aliasing error on all low-order modes due to each high-order mode. For example, the value at mode 20 is the aliasing error due to modes 5 to 20 (the modes 0 to 4 are the ones we want to correct). Computed from high-order residuals at 70" off-axis, with a WCoG of FWHM = 2 pixels. Pixel scale: 10 mas (2×2) or 20 mas (others).

We do not retrieve the classical result, which shows that better pupil sampling reduces aliasing effects. This result would be found with a normal center of gravity and estimating more modes when increasing the number of subapertures. The source of the difference here is mainly the slope computation with the WCoG, which acts as a spatial filter in the subaperture focal plane. Estimating more modes with the WCoG leads to similar results.

Hence, there is no strong advantage in choosing a configuration rather than another. We can therefore assume all pupil samplings have a similar behavior with respect to aliasing, and focus on the noise error to choose the optimal configuration.

2.1.6 Choice of the configuration

We now compare the performance of different configurations with respect to the detected flux (Fig. 6). There is a clear advantage using the infrared light, even at 85" off-axis. The best performance is obtained with the SH 2×2. In this analysis, we have found that the pixel of 10 mas is the best fitted for the SH 2×2 in infrared (with low difference with greater pixel sizes).
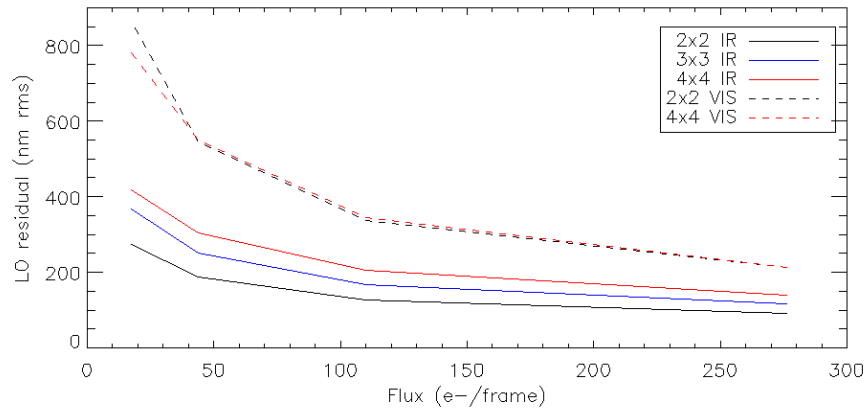
Figure 6. Theoretical closed-loop residual due to noise for different pupil samplings, in visible or infrared. The NGS in infrared is considered at 85" off axis. The loop gain is always 0.2 and the WCoG's FWHM is always 2 pixels. In infrared, the Strehl ratio is 0.06, meaning that the flux is scaled by 0.06 before making the image. The SH 2×2 in infrared has 10 mas pixels, the 3×3 and 4×4 have 20 mas pixels. In visible, all configurations have 100 mas pixels. Readout noise: 0.8 e- in infrared, 0.375 e- in visible. Dark current: 0.04 e-/pixel/frame in infrared, 0.006 e-/pixel/frame in visible. Background on the SH 2×2: 0.157 e-/frame/pixel in infrared, 0.387 e-/frame/pixel in visible (scaled with pupil sampling and pixel size in other configurations).

In the following, we thus consider the SH 2×2 in H band with a 10 mas pixel as the baseline for the LO sensors design.

3. SKY COVERAGE

In this section, we present the first assessment of sky coverage, computed from the galaxy model TRILEGAL[5] and the end-to-end simulation code PASSATA.[6]

The goal of this study is to define the main parameters of the MCAO system, such as the number of Post-Focal DMs (PFDM) or the technical FoV size, by comparing the different configurations with respect to the sky coverage requirement. This requirement is defined as follows: MAORY should have a 50% probability of providing a SR of 30% at 2200 nm over a FoV of 1' diameter under median atmospheric conditions. As a first step, we consider only the SR on axis.

We also consider the option of using a specific DM in the path of the LO sensor (so-called Dual AO[7]), that would be controlled in open-loop to correct around 100 modes in the direction of the NGS, and thus enhance the LO sensor's performance. This is motivated by the low Strehl ratios seen far off-axis when using a single PFDM.

3.1 Method

3.1.1 Asterism catalog generation

From TRILEGAL, we get a list of stars in a $3 \times 3°$ field at the South Galactic Pole. These stars are placed with a uniform probability. We then generate a series of random pointing coordinates. For each pointing, we register all asterisms that are geometrically valid with respect to the technical FoV size, the pick-off mirror size and the overlap between sensors. Fields with only 1 or 2 stars are also registered.

3.1.2 LO residual computation

For each asterism, we compute the LO residual on axis from the following equation:

$$\sigma_{LO} = \sqrt{\sigma_{wind}^2 + \sigma_{tomo}^2 + \text{Tr}(RC_{nn}R^t)} \tag{11}$$

where σ_{wind}^2 is the residual tip/tilt vibration due to windshake on the telescope, σ_{tomo}^2 is the pure tomographic error due to the asterism geometry, R is the reconstruction matrix and C_{nn} is the noise covariance matrix of

the 3 NGSs. The latter is considered diagonal and the noise on each mode of each star is approximated by the average noise on the 5 LO modes. We consider here that aliasing and temporal errors are part of the noise.

The windshake residual and pure tomographic error computation are respectively explained in Appendices B and C. The noise error is derived from PASSATA simulations, with the following parameters:

- Median ESO profile with median seeing 0.644".

- DM altitudes: 5 and 15.5 km. Only the highest is kept in the 1 PFDM case.

- LGSs at 45".

- Optimized FoV radius = 30" (so-called FoV of interest in Fusco et al.[8]).

- No LGS spot elongation.

A full MCAO simulation is performed for several equilateral asterisms with all stars at the same distance and magnitude. The distances range from 55" (minimum due to MICADO's FoV and the pick-off mirror size) to 100" (maximum considered radius for the technical FoV) and the magnitudes from H=10 to H=21. The noise error for a given couple (distance, magnitude) is considered as the average LO residuals in the NGSs' directions in the MCAO closed loop. It is then interpolated for any distance and magnitude.

In the following, we assume that the brightest star of the asterism is sensed at 500 Hz, in order to efficiently correct windshake, while the other stars are sensed at 100 Hz, that is sufficient for turbulence compensation. This way, we can ensure a greater limiting magnitude than with a synchronous sensing at 500 Hz.

3.1.3 Sky coverage computation

The best residual obtained on each field is registered. We then compute the sky coverage as the ratio between the number of fields giving a residual lesser or equal to a given value and the total number of fields:

$$SC(x) = \frac{\sum_i P_i(\sigma_{LO} \leqslant x)}{N_{fields}} \tag{12}$$

with $P_i(\sigma_{LO} \leqslant x) = 1$ if the i-th field has an asterism giving a residual lesser than x and $P_i(\sigma_{LO} \leqslant x) = 0$ otherwise.

3.2 Sky coverage for different configurations

We plot in Fig. 7 the sky coverage for different FoV sizes, with 1 or 2 PFDMs. The SR is computed from the LO residuals given by the sky coverage analysis, added to a constant residual corresponding to 220 nm of high orders (derived from the simulations) and 145 nm of contingency (from MAORY specifications).
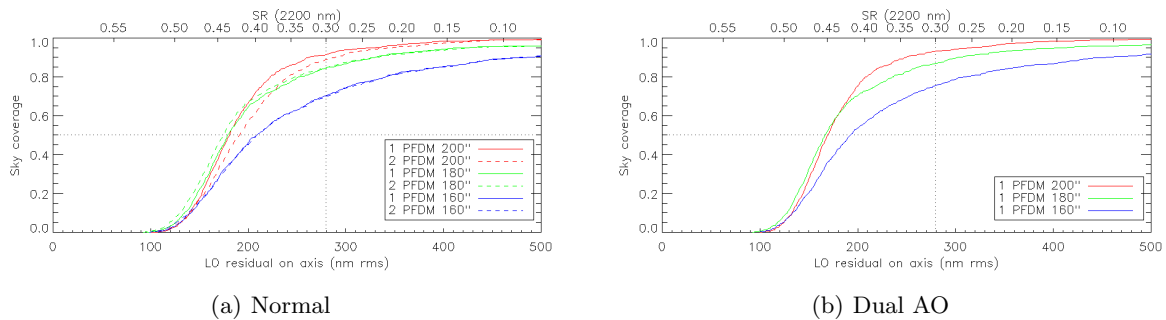

Figure 7. Sky coverage as a function of LO residuals and SR for all the considered FoV sizes. Left: without Dual AO. Right: with Dual AO. The magnitude is limited to H=22. The SR is computed assuming a high-order residual of 220 nm and 145 nm of contingency.

We see that all configurations are above the requirement (30% SR with 50% sky coverage), meaning that 1 PFDM is sufficient. The 2 PFDMs even perform worse than the 1 PFDM alone for the FoV 200". This is due to the FoV optimization: in the outer part of the technical FoV, the 2 PFDMs perform worse than the 1 PFDM alone for the chosen optimized FoV radius (other configurations are under study). This effect disappears when reducing the FoV, as the selected NGSs are less far from the axis. If one still wants to have the performance of the 2 PFDMs (for risk mitigation), it can be obtained using the Dual AO. This can be an interesting solution in terms of complexity and cost.

From this analysis, one could choose the FoV of 160", but the error budget is still lacking some terms (no LGS truncation, no non-common path aberrations...), so this configuration might be discarded in the future. From now on, the baseline will be 180", as it gives a result very similar to the FoV of 200". The 160" FoV solution will still be investigated, as it might provide a significant improvement of the optical design, leading to smaller residuals in the full FoV.

4. CONCLUSION

Through a semi-analytical study, we have determined the parameters of the LO sensors design: 2×2 subapertures, sensing in H band, with ∼10 mas pixels (Nyquist sampling of the subaperture spot). From this design, and using a combination of full MCAO end-to-end simulations and analytical formulas, we were able to compute the performance of MAORY for any NGS asterism, and thus derive the sky coverage from the galaxy model TRILEGAL. The sky coverage study showed that we should set the technical FoV size to 180", and that 1 PFDM would be sufficient to provide the required performance. We also noted that having a dedicated DM in the LO sensor's path could improve the performance to the same level as a 2-PFDM configuration. This solution could be considered in the future if the error budget becomes higher than expected.

In this paper, we have computed the sky coverage with Strehl ratios on axis and with a simplified error budget. Future works will focus on calculating the Strehl ratio on the full MICADO FoV and redefining the error budget to have more realistic numbers.

APPENDIX A. COMPUTATION OF THE STATISTICS OF A PIXEL THRESHOLDED AT 0

The noise on each pixel is the sum of a Poisson noise (incoming flux, background and dark current) and a zero-mean Gaussian noise (read-out). We consider that the background and dark current are not removed here. The Poisson noise, by nature, is not affected by the threshold at 0. The only effect of this threshold is then to truncate the read-out noise probability distribution at a value $-f_k$, the average flux on the pixel k (star + background + dark current). This means that, without the Poisson noise, the probability of having negative pixels is 0. This is of course an approximation, as the flux on the pixel k oscillates around f_k. The mean and variance of each pixel value is the sum of the means and variances of the Poisson noise and the truncated Gaussian noise. We thus need to compute the mean and variance of the truncated Gaussian noise. The mean is:

$$\mu_{G,thr} = \frac{1}{\sqrt{2\pi\sigma_e^2}} \int_{-f_k}^{\infty} x e^{-\frac{x^2}{2\sigma_e^2}} dx = \frac{1}{\sqrt{2\pi\sigma_e^2}} \left[-\sigma_e^2 e^{-\frac{x^2}{2\sigma_e^2}} \right]_{-f_k}^{\infty} \tag{13}$$

$$\mu_{G,thr} = \sigma_e \varphi\left(-\frac{f_k}{\sigma_e} \right) \tag{14}$$

with σ_e the read-out noise standard deviation and $\varphi(x) = \frac{1}{\sqrt{2\pi}} e^{-\frac{x^2}{2}}$. The variance is:

$$\sigma_{G,thr}^2 = \frac{1}{\sqrt{2\pi\sigma_e^2}} \int_{-f_k}^{\infty} x^2 e^{-\frac{x^2}{2\sigma_e^2}} dx - \mu_{G,thr}^2 \tag{15}$$

To compute the integral, we use an integration by parts with:

$$u = x \rightarrow u' = 1$$
$$v' = x e^{-\frac{x^2}{2\sigma_e^2}} \rightarrow v = -\sigma_e^2 e^{-\frac{x^2}{2\sigma_e^2}} \tag{16}$$

That gives:

$$\frac{1}{\sqrt{2\pi\sigma_e^2}} \int_{-f_k}^{\infty} x^2 e^{-\frac{x^2}{2\sigma_e^2}}\, dx = \frac{1}{\sqrt{2\pi\sigma_e^2}} \left[-x\sigma_e^2 e^{-\frac{x^2}{2\sigma_e^2}} \right]_{-f_k}^{\infty} + \frac{\sigma_e^2}{\sqrt{2\pi}} \int_{-f_k}^{\infty} e^{-\frac{x^2}{2\sigma_e^2}} \tag{17}$$

$$\frac{1}{\sqrt{2\pi\sigma_e^2}} \int_{-f_k}^{\infty} x^2 e^{-\frac{x^2}{2\sigma_e^2}}\, dx = -f_k \sigma_e \varphi\left(-\frac{f_k}{\sigma_e}\right) + \sigma_e^2 \left[1 - \Phi(-f_k)\right] \tag{18}$$

with $\Phi(x) = \frac{1}{2}\left[1 + \text{erf}\left(\frac{x}{\sqrt{2}}\right)\right]$, erf being the error function. We used here the fact that $\lim\limits_{x\to\infty} x e^{-\frac{x^2}{2\sigma_e^2}} = 0$, that can be demonstrated using the L'Hopital theorem. In the end, the variance can be expressed as:

$$\sigma_{G,thr}^2 = \sigma_e^2 \left[1 - \Phi(-f_k) - \varphi\left(-\frac{f_k}{\sigma_e}\right)^2 \right] - f_k \sigma_e \varphi\left(-\frac{f_k}{\sigma_e}\right) \tag{19}$$

Finally, we can express the final mean and variance of the pixel k, for an excess noise factor F:

$$\mu_{k,thr} = f_k + \sigma_e \varphi\left(-\frac{f_k}{\sigma_e}\right) \tag{20}$$

$$\sigma_{G,thr}^2 = F f_k + \sigma_e^2 \left[1 - \Phi(-f_k) - \varphi\left(-\frac{f_k}{\sigma_e}\right)^2 \right] - f_k \sigma_e \varphi\left(-\frac{f_k}{\sigma_e}\right) \tag{21}$$

APPENDIX B. COMPUTATION OF WINDSHAKE ERROR

The secondary mirror (M2) of the ELT will be close to the dome aperture and thus undergo a rather strong wind in some cases, causing high-amplitude vibrations. ESO provided the first-light instruments consortia with a "data package", in which one can find a 300 seconds time series of the wavefront tip/tilt due to such a "windshake". This time series corresponds to a worst case scenario: external wind 10 m/s (scenario), wind in the dome 8 m/s (scenario), frontal wind w.r.t. the telescope (worst condition), telescope zenith distance pointing 45° (worst condition for frontal wind), wind screen deployed up not to vignette the telescope aperture (normal operating setup). The temporal PSDs of the tip and tilt corresponding to the time series are plotted in Fig. 8.
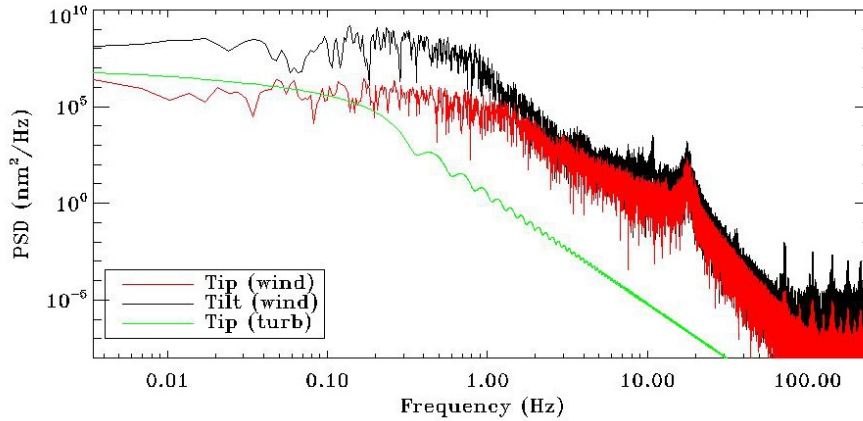

Figure 8. Temporal PSDs of the tip/tilt due to the windshake on M2, compared to the turbulence PSD. The PSDs are computed from the time series using a Hanning window.

We consider here that the windshake will be corrected by MAORY, without using the probes of the telescope (that will normally do a first-step correction). To compute the expected residuals, we apply a temporal filter on the PSD, assuming a certain level of noise. The residual is then:

$$\text{MSE} = \int_0^{\infty} \left[|\text{RTF}|^2\, \text{PSD}_{\text{wind}} + |\text{NTF}|^2\, \text{PSD}_{\text{noise}} \right] df \tag{22}$$

with RTF the Rejection Transfer Function and NTF the Noise Transfer Function corresponding to the temporal filter. The noise PSD is defined as in Eq. 7, and the noise level is derived from section 2.1.2, assuming a 2-pixel FWHM for the WCoG (∼ diffraction-limited spot FWHM) and a Strehl ratio of 11%.

The order of the temporal filter was set to 2, as there is much energy at low frequencies (higher orders did not show a significant improvement). The poles and zeros of the filter were then optimized for each magnitude, or noise level, to give the residuals shown in Table 1. Those residuals (interpolated at the correct magnitude) are the ones used in the sky coverage computation. We recall that the sensing frequency for the windshake is 500 Hz.

Table 1. Windshake residual error. 1 mas = 47 nm rms.

H mag.	Windshake (nm rms)		Noise (1 axis, nm rms)	Residual (nm rms)		
	Tip	Tilt		Tip	Tilt	Total
10			4	5.4	8.5	10
15			55	24.4	42.2	48.8
16			96	34.6	59.5	68.9
17	596	12958	203	57.5	96	111.9
18			427	99	162.3	190.1
18.5			615	124.8	212	246
19.5			1301	201.4	382.1	432

APPENDIX C. COMPUTATION OF TOMOGRAPHIC ERROR

The goal of this appendix is to compute the LO residual on axis due to the tomographic reconstruction error. We assume that we will perform a split tomography in MAORY, meaning that the high-order (modes after astigmatism, sensed with the LGSs) and low-order modes (tip/tilt, focus and astigmatism, sensed from the NGSs) will be estimated separately. We can thus assess the tomographic error using the NGSs only. The method developed here is inspired from what has been done for the GMT and HARMONI. We can write the estimation of the LO modes on axis as:

$$\hat{a} = R(s + n) \tag{23}$$

with a the vector of LO modes coefficients on axis, s the vector grouping all the measured LO modes coefficients for all NGSs, n the noise on these measurements and R the reconstructor. We define here the reconstructor as:

$$R = P_0 W \tag{24}$$

with P_0 the projection on axis and W the tomographic reconstructor, computed with 2 layers (all LO modes on ground layer and focus/astigmatism on altitude layer). The covariance matrix of the LO modes on axis can then be expressed as (assuming the noise is not correlated with a or s):

$$< (a - \hat{a})(a - \hat{a})^t > = C_{aa} - C_{as}R^t - RC_{as}^t + RC_{ss}R^t + RC_{nn}R^t \tag{25}$$

with $C_{xy} = < xy^t >$ the covariance between x and y. The formula to compute these covariance matrices for Zernike modes is given in Appendix D. We can finally define the tomographic error as:

$$\sigma_{tomo,tot} = \sqrt{\sigma_{tomo,0}^2 + \sigma_{tomo,n}^2} \tag{26}$$

with

$$\sigma_{tomo,0}^2 = C_{aa} - C_{as}R^t - RC_{as}^t + RC_{ss}R^t \tag{27}$$

the pure tomographic error and

$$\sigma_{tomo,n}^2 = RC_{nn}R^t \tag{28}$$

the tomographic noise error.

APPENDIX D. COMPUTATION OF ZERNIKE MODES COVARIANCES

The covariance between 2 Zernike mode coefficients a_j and a_k (in Noll's definition[9]), in the direction of 2 different stars at coordinates $\vec{\theta_1}$ and $\vec{\theta_2}$ is, for a telescope of radius R:[10]

$$
< a_j\left(\vec{\theta_1}\right) a_k\left(\vec{\theta_2}\right) > = (-1)^{m_k}\sqrt{(n_j+1)(n_k+1)}i^{n_j+n_k}2^{1-0.5(\delta_{0m_j}+\delta_{0m_k})}\int dh \frac{1}{\pi R^2\left(1-\frac{h}{z_1}\right)\left(1-\frac{h}{z_2}\right)}
$$

$$
\times \int_0^\infty \frac{df}{f}W_\varphi(h,f)J_{n_j+1}\left(2\pi fR\left(1-\frac{h}{z_1}\right)\right)J_{n_k+1}\left(2\pi fR\left(1-\frac{h}{z_2}\right)\right)
$$

$$
\times \left\{ cos\left((m_j+m_k)arg\left(\vec{\theta_1}-\vec{\theta_2}\right)+\frac{\pi}{4}\left((1-\delta_{0m_j})\left((-1)^j-1\right)+(1-\delta_{0m_k})\left((-1)^k-1\right)\right)\right)\right.
$$

$$
\times i^{3(m_j+m_k)}J_{m_j+m_k}\left(2\pi fh|\vec{\theta_1}-\vec{\theta_2}|\right)
$$

$$
+cos\left((m_j-m_k)arg\left(\vec{\theta_1}-\vec{\theta_2}\right)+\frac{\pi}{4}\left((1-\delta_{0m_j})\left((-1)^j-1\right)-(1-\delta_{0m_k})\left((-1)^k-1\right)\right)\right)
$$

$$
\left. \times i^{3|m_j-m_k|}J_{|m_j-m_k|}\left(2\pi fh|\vec{\theta_1}-\vec{\theta_2}|\right)\right\}
$$

$$(29)$$

with n_j and m_j the radial and azimuthal orders of the j-th polynomial, δ_{0x} the Kronecker delta between 0 and x, h the layer altitude, z_1 and z_2 the altitudes of the 2 stars (= infinity for NGSs), $J_n(x)$ the Bessel function of first kind of order n, f the spatial frequency and $W_\varphi(h,f)$ the turbulent phase PSD for the layer at altitude h. The turbulent PSD used in this paper is the one defined by Von-Karman:

$$
W_\varphi(h,f) = 0.023r_0(h)^{-\frac{5}{3}}\left(f^2+\frac{1}{L_0^2}\right)^{-\frac{11}{6}}
$$

$$(30)$$

with r_0 the Fried parameter and L_0 the outer scale (= 25 m throughout the paper).

ACKNOWLEDGMENTS

REFERENCES

[1] Diolaiti, E. et al., "MAORY: adaptive optics module for the E-ELT," *SPIE Proceedings* (2016).

[2] Davies, R. et al., "MICADO: first-light imager for the E-ELT," *SPIE Proceedings* (2016).

[3] Le Louarn, M., Verinaud, C., Korkiakoski, V., Hubin, N., and Marchetti, E., "Adaptive optics simulations for the European Extremely Large Telescope," **6272**, 98– (07 2006).

[4] Thomas, S., Fusco, T., Tokovinin, A., Nicolle, M., Michau, V., and Rousset, G., "Comparison of centroid computation algorithms in a Shack–Hartmann sensor," *Monthly Notices of the Royal Astronomical Society* **371**(1), 323–336 (2006).

[5] Girardi, L., Barbieri, M., Groenewegen, M. A. T., Marigo, P., Bressan, A., Rocha-Pinto, H. J., Santiago, B. X., Camargo, J. I. B., and da Costa, L. N., "TRILEGAL, a TRIdimensional modeL of thE GALaxy: Status and Future," *Astrophysics and Space Science Proceedings* **26**, 165 (2012).

[6] Agapito, G., Puglisi, A., and Esposito, S., "PASSATA: object oriented numerical simulation software for adaptive optics," in [*Adaptive Optics Systems V*], **9909**, 99097E, International Society for Optics and Photonics (2016).

[7] Rigaut, F. and Gendron, E., "Laser guide star in adaptive optics-The tilt determination problem," *Astronomy and Astrophysics* **261**, 677–684 (1992).

[8] Fusco, T., Conan, J.-M., Rousset, G., Mugnier, L. M., and Michau, V., "Optimal wave-front reconstruction strategies for multiconjugate adaptive optics," *J. Opt. Soc. Am. A* **18**, 2527–2538 (Oct 2001).

[9] Noll, R. J., "Zernike polynomials and atmospheric turbulence," *Opt. Soc. Am.* **66** (1976).

[10] Whiteley, M. R., Roggemann, M. C., and Welsh, B. M., "Temporal properties of the Zernike expansion coefficients of turbulence-induced phase aberrations for aperture and source motion," *J. Opt. Soc. Am. A* **15**, 993–1005 (Apr 1998).